Eur. Phys. J. B **44**, 183–188 (2005)
DOI: 10.1140/epjb/e2005-00113-8

THE EUROPEAN PHYSICAL JOURNAL B

Anisotropy of the upper critical field in MgB_2: the two-gap Ginzburg-Landau theory

V.H. Dao[a] and M.E. Zhitomirsky

Commissariat à l'Énergie Atomique, DSM/DRFMC/SPSMS, 17 avenue des Martyrs, 38054 Grenoble Cedex 9, France

Received 26 August 2004 / Received in final form 26 January 2005
Published online 20 April 2005 –

Abstract. The upper critical field in MgB_2 is investigated in the framework of the two-gap Ginzburg-Landau theory. A variational solution of linearized Ginzburg-Landau equations agrees well with the Landau level expansion and demonstrates that spatial distributions of the gap functions are different in the two bands and change with temperature. The temperature variation of the ratio of two gaps is responsible for the upward temperature dependence of in-plane H_{c2} as well as for the deviation of its out-of-plane behavior from the standard angular dependence. The hexagonal in-plane modulations of H_{c2} can change sign with decreasing temperature.

PACS. 74.70.Ad Metals; alloys and binary compounds (including A15, MgB2, etc.) – 74.20.De Phenomenological theories (two-fluid, Ginzburg-Landau etc.) – 74.25.Op Mixed states, critical fields, and surface sheaths

1 Introduction

Multigap superconductivity [1,2] has been discussed in the late 1950's for materials with a varying strength of electron-phonon interactions between different pieces of the Fermi surface. After the discovery of superconductivity in MgB_2 [3] in 2001, an impressive collection of experimental and theoretical works [4] has established that this compound is the first unambiguous example of a multigap superconductor. In MgB_2 the charge carriers are distributed between two sets of bands: the σ-bands with quasi-2D cylindrical Fermi sheets and the π-bands with 3D sheets forming a tubular network. The electron-phonon coupling is stronger in the σ-bands than in the π-bands, and gives rise to an s-wave phonon-mediated superconductivity with two gaps $\Delta_1 \sim 7$ meV and $\Delta_2 \sim 2.5$ meV. Since the two sets have different characteristics (interaction with phonons, geometry of the Fermi sheets, impurity dependence etc.), an interplay between them results in deviations from the standard BCS theory. The most striking consequences of the two gaps are the unusual anisotropic features of MgB_2 under magnetic field, for example, inequality between the penetration depth and the upper critical field anisotropies, and their variations with temperature [5–16], and the 30°-reorientation of the flux line lattice with increasing magnetic field applied along the c-axis [17,18].

The two-gap Ginzburg-Landau (GL) theory for MgB_2 developed in reference [18] (see also the preceding works [19,20]) is the exact limit of the microscopic theory in the vicinity of the transition temperature. It can thus account for most of the observed properties in a clear and coherent way near T_c, while its simplicity compared to earlier studies is useful to understand the physics in this material. In the present paper we extend our previous analysis of the two-band effects [18] on angular and temperature dependence of the upper critical field H_{c2}. We minimize the GL functional using a variational procedure, which highlights separate spatial anisotropies of the gap in each band. This is an improvement compared to the earlier solutions where only one common distortion for both gaps is considered [11,14]. This method is compared to a solution based on the Landau level expansion. We then estimate the temperature range of the GL regime. The present study covers the out-of-plane H_{c2} anisotropy. By going beyond the ellipsoid Fermi sheet approximation of references [12,14], we also calculate in-plane modulation of the upper critical field arising from the hexagonal crystal symmetry.

For a clean two-band BCS superconductor with two gaps Δ_1 and Δ_2, the GL functional [18] has the form

$$F_{GL} = \int dx \Big[\alpha_1|\Delta_1|^2 + \alpha_2|\Delta_2|^2 - \gamma(\Delta_1^*\Delta_2 + \Delta_2^*\Delta_1) + K_{1i}|\Pi_i\Delta_1|^2 + K_{2i}|\Pi_i\Delta_2|^2 + \tfrac{1}{2}\beta_1|\Delta_1|^4 + \tfrac{1}{2}\beta_2|\Delta_2|^4\Big],$$
$$\Pi_i = -i\partial_i + \frac{2\pi}{\Phi_0}A_i, \quad \alpha_{1,2} = \frac{g_{2,1}}{G} - N_{1,2}\ln\frac{2\omega_D e^C}{\pi T},$$
$$\gamma = \frac{g_3}{G}, \quad K_{ni} = \frac{7\zeta(3)N_n}{16\pi^2 T_c^2}\left\langle v_{Fni}^2\right\rangle, \quad \beta_n = \frac{7\zeta(3)N_n}{8\pi^2 T_c^2} \quad (1)$$

[a] e-mail: dao@drfmc.ceng.cea.fr

where repeating index i implies a sum, Φ_0 is the quantum flux, $\mathbf{A}$ the potential vector, g_1 and g_2 the intraband pairing coefficients ($n = 1{,}2$ for the σ,π-band), g_3 the interband pairing coefficient, $G = g_1 g_2 - g_3^2$, N_n the density of states at the Fermi level in the band n, ω_D the Debye frequency, C the Euler constant, and $\langle v_{Fni}^2 \rangle$ the square of the Fermi velocity i-component averaged on the sheet n. It is then convenient to write $\alpha_1 = -a_1 t$ with $a_1 = N_1$, $t = \ln(T_1/T)$ and $T_1 = (2\omega_D e^C/\pi) e^{-g_2/GN_1}$ for the first active band and $\alpha_2 = \alpha_{20} - a_2 t$ with $a_2 = N_2$ for the passive band. In MgB_2 the active and passive bands correspond to the σ and π bands, respectively.

The crystal structure of MgB_2 is uniaxial, so the gradient coefficients are the same for all directions in the basal plane, and $K_{na} = K_{nb} = K_n$. LDA calculations [21] yield for the highly anisotropic σ-band $\langle v_{F1ab}^2 \rangle = 2.13$ and $\langle v_{F1c}^2 \rangle = 0.05$, while for the π-band $\langle v_{F2ab}^2 \rangle = 1.51$ and $\langle v_{F2c}^2 \rangle = 2.96$, all numbers are in units of 10^{15} cm^2/s^2. With the provided ratio $N_2/N_1 = 1.5$, the in-plane gradient constants for the two bands are practically the same $K_2/K_1 \approx 1.06$, whereas the c-axis constants differ by almost two orders of magnitude $K_{2c}/K_{1c} \approx 90$. A crude estimate for H_{c2} at zero temperature by $\frac{N_1}{\sqrt{K_1 K_{1c}}} \frac{\Phi_0}{2\pi} \approx 4$ T is substantially smaller than the experimental value $H_{c2}^{ab}(0\text{ K}) \approx 18$ T, which suggests the gradient constants based on LDA data are over-estimated by a factor of four. Such a discrepancy is due to a significant renormalization of effective masses by the electron-phonon coupling. The electron-phonon coupling leads to effective masses twice larger than the LDA prediction in the σ-band, whereas they are only slightly renormalized in the π-band [22]. The reduction of gradient term coefficients is given by squares of the mass renormalization factors.

The interband impurity scattering in MgB_2 is exceptionally small due to its particular electronic structure, even in low quality samples [23]. The clean limit two-gap GL theory described above is straightforwardly extended to include the effect of s-wave intraband scattering by nonmagnetic impurities [24]: the GL functional keeps the same form wherein the expression for K_{ni} has to be replaced by $K_{ni} = \pi N_n \langle v_{Fni}^2 \rangle \Lambda(\tau_n)/8T_c$ with

$$\Lambda(\tau_n) = \tau_n \frac{8}{\pi^2} \sum_m \frac{1}{(2m+1)^2((2m+1)2\pi\tau_n T_c + 1)}, \quad (2)$$

where τ_n is the transport collision time in the band n. The intraband anisotropy is then the same as in the clean limit, while the renormalization factor $\Lambda(\tau_n)$ can vary between the two bands due to different sensitivity to impurities. The resulting GL equations are naturally found as the limit of Usadel equations near T_c [11,15].

2 Upward curvature of $H_{c2}^{ab}(T)$

In this section the z-axis is fixed along the crystal c-axis and the y-axis is taken parallel to the magnetic field applied in the ab-plane. The vector potential is chosen in the Landau gauge as $\mathbf{A} = (Hz, 0, 0)$. The coupled linearized GL equations for solutions homogeneous along the field direction are

$$\left(\alpha_n + K_n h^2 z^2 - K_{nc}\partial_z^2\right) \Delta_n - \gamma \Delta_{n'} = 0 \quad (3)$$

for $n = 1, 2$, $n' = 2, 1$, with the reduced magnetic field $h = 2\pi H/\Phi_0$. Since $K_{1c}/K_1 \neq K_{2c}/K_2$, an analytic solution can not be obtained by rescaling distances as in the single-gap case. We, therefore, search for an approximate solution of the form

$$\begin{pmatrix} \Delta_1 \\ \Delta_2 \end{pmatrix} = \begin{pmatrix} c\,\tilde{\xi}_1^{-\frac{1}{2}} \Psi_0(z/\tilde{\xi}_1) \\ d\,\tilde{\xi}_2^{-\frac{1}{2}} \Psi_0(z/\tilde{\xi}_2) \end{pmatrix} \quad (4)$$

where the Landau level wave functions are defined by

$$\Psi_p(z) = \frac{1}{\sqrt{p!}} \left[\frac{1}{\sqrt{2}}(-\partial_z + z)\right]^p \frac{e^{-z^2/2}}{\pi^{1/4}}. \quad (5)$$

Different coherence lengths for each band are allowed with the parameterization $\tilde{\xi}_n^2 = \mu_n/h$ where μ_n quantifies the distortion of the spatial distribution of the nth component (in the single-gap case, μ is the stretching factor of the flux line lattice at the upper critical field and is independent from temperature). The following quadratic form in the GL functional is then found:

$$F_2 = \left(\alpha_1 + h\tilde{K}_1\right)|c|^2 + \left(\alpha_2 + h\tilde{K}_2\right)|d|^2 - \tilde{\gamma}\,(c^* d + d^* c) \quad (6)$$

with $\tilde{K}_n = \frac{1}{2}(K_n \mu_n + K_{nc}/\mu_n)$ and $\tilde{\gamma}^2 = \gamma^2 \frac{2\sqrt{\mu_1\mu_2}}{\mu_1+\mu_2}$. At the transition field, the determinant in equation (6) vanishes. This condition leads to

$$\tilde{h}(\mu_1, \mu_2) = -\frac{\alpha_1}{2\tilde{K}_1} - \frac{\alpha_2}{2\tilde{K}_2} + \sqrt{\left(\frac{\alpha_1}{2\tilde{K}_1} - \frac{\alpha_2}{2\tilde{K}_2}\right)^2 + \frac{\tilde{\gamma}^2}{\tilde{K}_1\tilde{K}_2}}. \quad (7)$$

In order to find the (nucleation) upper critical field, $\tilde{h}$ is maximized $\tilde{h}_{c2} = \max_{\mu_1,\mu_2} \tilde{h}(\mu_1, \mu_2)$.

Within the above variational scheme, the analytic expressions for the in-plane transition field are possible in two temperature regimes. Near T_c, vanishing $\tilde{h}$ implies that the superconducting gaps have the same variation length in each band. The condition $\mu_1 = \mu_2$ yields

$$\tilde{h}_{c2}^{ab} \approx \frac{a_1(t - t_c)}{\sqrt{(K_1 + \rho^2 K_2)((K_{1z} + \rho^2 K_{2z})}} \quad (8)$$

with the gap ratio $\rho = |d/c| \approx \sqrt{\alpha_1/\alpha_2}$ and $t_c = \ln(T_1/T_c)$. Since $K_{1c} \sim 0.01 K_{2c}$ in MgB_2, whereas $\rho^2 \approx 0.1$, we can simplify the above expression to

$$\tilde{h}_{c2}^{ab} \approx \frac{a_1(t - t_c)}{\rho\sqrt{K_1 K_{2c}}}. \quad (9)$$

In the second temperature regime for $T < T_1$, the first active band is dominant and

$$\tilde{h}_{c2}^{ab} \approx \frac{a_1 t}{\sqrt{K_1 K_{1c}}}. \quad (10)$$

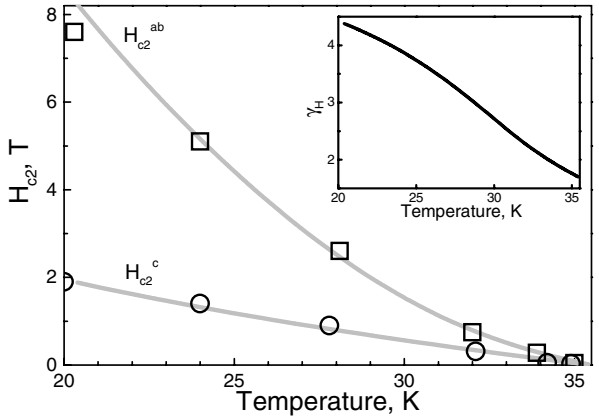

Fig. 1. The upper critical field in MgB_2: experimental data from Lyard et al. [6] (symbols) and the GL computations with parameters $\alpha_{20} = 0.65a_1$ and $\gamma = 0.4a_1$ (solid lines). The inset shows the anisotropy ratio $\gamma_H = H_{c2}^{ab}/H_{c2}^{c}$.

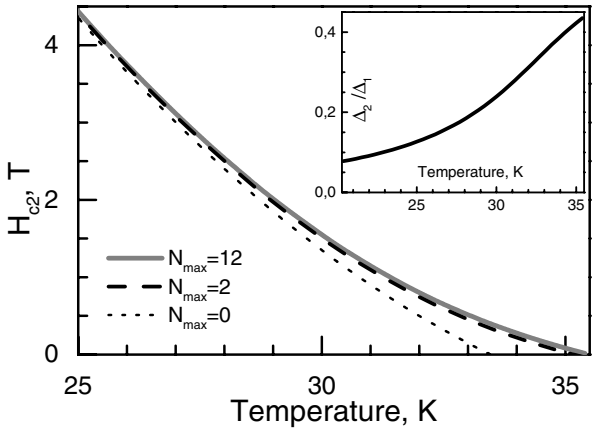

Fig. 2. In-plane H_{c2} calculated with the Landau level expansion to the order $N_{\max}$ for the same parameters as in Figure 1. The inset displays the gap ratio $\rho = \Delta_2/\Delta_1$ found with the highest expansion order.

The line $H_{c2}^{ab}(T)$ exhibits, therefore, a marked upturn curvature between the two regimes, in contrast to H_{c2}^{c}(T). The two upper critical fields are plotted in Figure 1. In order to fit the experimental data, we have renormalized all gradient constants obtained from the LDA data by a factor of five. The corresponding mass enhancement $\sqrt{5} \approx 2.2$ roughly agrees with the electron-phonon renormalization factor [22]. For simplicity, the same value has been applied for both bands.

In order to verify an accuracy of the variational method, we alternatively proceed by expanding the gap functions in terms of the the Landau levels: $\Delta_n = \sum_p c_{n,p}\phi_{n,p}$ where $\phi_{n,p}(z) = \xi_n^{-1/2}\Psi_p(z/\xi_n)$ and $\xi_n^2 = \sqrt{K_{nc}/K_n}/h$. For the upper critical field this expansion is restricted to the even order levels. The quadratic part of the GL functional has the following matrix element in this base:

$$M^{F_2}_{2p+n,2q+n'} = \left(\alpha_n + (4p+1)h\sqrt{K_n K_{nc}}\right)\delta_{n,n'}\delta_{p,q}$$
$$-\gamma\int dx\ \phi^*_{n,2p}(x)\phi_{n',2q}(x)\ (1-\delta_{n,n'}) \qquad (11)$$

with $n, n' \in \{1, 2\}$, and $p, q \geq 0$. The upper critical field h_{c2} is then approximated by the largest root of the sub-matrix determinant corresponding to the desired expansion up to the order $N_{\max}$.

Although the zeroth order approximation significantly deviates near T_c (see Fig. 2), the procedure is rapidly converging with increasing the expansion order, even in the case of a great disparity between the two bands (e.g., $\xi_1^2/\xi_2^2 \geq 100$ or ≤ 0.01). The expansion to the order $N_{\max} \geq 12$ yields the upper critical field curve in excellent agreement with the variational solution (the two curves are indistinguishable on the scale of Fig. 2).

Figure 3 displays the behavior of the parameters μ_n defining the effective anisotropy of the variation lengths $\tilde{\xi}_n$ in the plane perpendicular to the magnetic field, i.e. $\mu_n = \tilde{\xi}_{nc}/\tilde{\xi}_{nab}$ for the magnetic field applied in the basal plane. This confirms the above analytic predictions: the

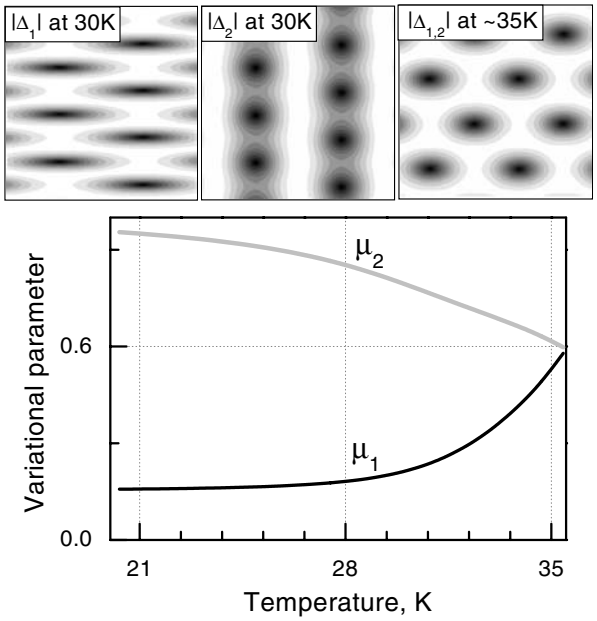

Fig. 3. Lower panel: temperature dependence of variational parameters for in-plane magnetic field and the same set of GL parameters as in Figure 1; Upper panel: absolute values of the two gaps in the vicinity of H_{c2} near to and away from the transition temperature.

order parameter varies on different length scales for each band, and μ_n can change with temperature contrary to the single-gap case. At T_c, the two parameters have the same value $\sqrt{(K_{1z} + \rho^2 K_{2z})/(K_1 + \rho^2 K_2)} = 0.59$ with $\rho = 0.44$, while $\mu_1 \approx \sqrt{K_{1c}/K_1} = 0.15$ below $T_1 = 29$ K. We should stress that periodic vortex structures for the two gaps have the same lattice parameters for arbitrary ratio of μ_1/μ_2. However, spatial distributions of $|\Delta_1(r)|^2$ and $|\Delta_2(r)|^2$ become quite different at low temperatures once $\mu_1 \ll \mu_2$. Such a behavior is demonstrated on the top panel of Figure 3. The different spatial distributions of the two gaps can be probed by scanning tunneling

microscopy. Also, magnetic field generated by superconducting currents $h_s(r) \sim (|\Delta_1(r)|^2 + |\Delta_2(r)|^2)$ should deviate significantly for a distribution expected for an anisotropic single-gap superconductor. Muon spin relaxation measurements can in principle verify such a behavior.

We shall now estimate the temperature range of the GL regime from the above computations. The gradient expansion is valid as long as $|K_{ni}\partial_i^2\Delta_n| < \Delta_n$ for all n and i. This condition is approximately replaced with $K_{ni}/\tilde{\xi}_{ni}^2 < 1$. The most restrictive case is for $K_{2c}/\tilde{\xi}_{2c}^2 = K_{2c}h_{c2}^{ab}/\mu_2$, which becomes $\sim$1 below $\sim$30 K, well beyond a narrow temperature regime suggested for the GL theory by Golubov and Koshelev [11]. The discrepancy is partially terminological, since in reference [11] the GL approximation always corresponds to an effective (anisotropic) single-gap GL theory, which is correct only when the ratio of the two gaps is constant. As we have demonstrated above, the full two-gap GL theory is valid in a much wider temperature range and describes adequately temperature variation of Δ_2/Δ_1 (Fig. 2) and of the two coherence lengths (Fig. 3).

3 Angular dependence of out-of-plane H_{c2}

Let us now discuss the out-of-plane behavior of the upper critical field. In the single-gap anisotropic GL theory, when **H** is tilted from the c-axis by an angle θ, the upper critical field has an elliptic (effective mass) angular dependence

$$H_{\rm SAGL}(\theta,T) = \frac{H_{c2}^c(T)}{\sqrt{\cos^2(\theta) + \sin^2(\theta)\gamma_H^{-2}}}, \qquad (12)$$

where $\gamma_H = H_{c2}^{ab}/H_{c2}^c$ is a temperature independent constant $\sqrt{K_c/K_{ab}}$. Experimental measurements in MgB_2 have shown that not only γ_H changes with temperature (Fig. 1) but deviations from the elliptic angular dependence (12) grow with decreasing temperature [5,8,9]. Such a behavior has been reproduced within quasiclassical Usadel equations [11]. The methods we have employed for H_{c2}^{ab} are still valid to find $H_{c2}(\theta)$: one needs only to replace K_{nc} by an angular dependent $K_n(\theta) = \cos^2(\theta)K_n + \sin^2(\theta)K_{nc}$ in the previous formula. Expression (7) for $\tilde{h}$ shows that the deviation grows with the disparity between the $\tilde{K}_n(\theta)$, so it increases when departing from T_c. The deviations can be quantified by $\delta A(\theta) = 1 - (H_{c2}(\theta)/H_{\rm SAGL}(\theta))^2$. Figure 4 displays the maximum deviation $\delta A_{\max} = \max_\theta \delta A(\theta)$. The dashed line is obtained from the two-gap GL theory with the parameters used above to fit the H_{c2}-data by Lyard et al. [6] in Figure 1. The calculation qualitatively reproduces experimental data from Rydh et al. [9]: $\delta A_{\max}$ increases with decreasing temperature and then saturates. But a quantitative discrepancy appears below $0.9T_c$ and becomes important at lower temperature. This deviation can be partially explained by the fact that experimental results are strongly sample dependent. At the present, the origin of the discrepancy remains an opened question. The full line is obtained with a modified interband coupling $\gamma^\star = 0.3a_1$ and $K_{c2}^\star = K_{2c}/3$ corresponding to a smaller anisotropy in the π-band.

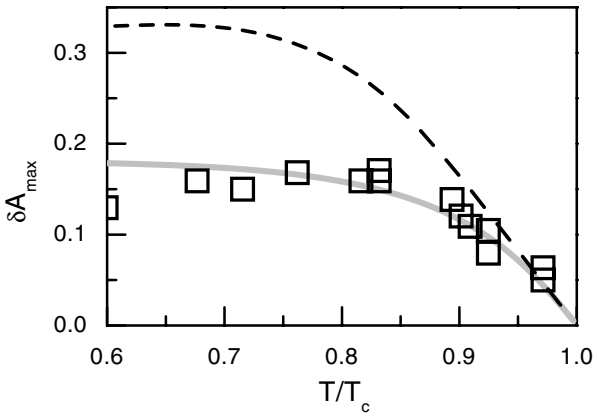

Fig. 4. Maximum deviation from the single-gap GL scaling law: squares are experimental data [9] and lines are obtained from the two-gap GL theory.

4 In-plane modulation of H_{c2}

In a hexagonal crystal, the transition magnetic field should exhibit a six-fold modulation when rotated about the c-axis [25]. The crystal field effect on superconductivity can be incorporated to the GL theory by including higher order (non-local) gradient terms [26]. Symmetry arguments suggest that coupling between the superconducting order parameter and the hexagonal crystal lattice appears at the sixth-order gradient terms. For a two-gap superconductor like MgB_2, the additional sixth-order part of the free energy is a sum of separate contributions from each band: $F_{GL} \longrightarrow F_{GL} + F_{6,1} + F_{6,2}$. The correction derived from the BCS theory [18,27] is (omitting the index $n = 1, 2$ for brevity)

$$F_6 = \frac{\zeta(7)N}{32\pi^6 T_c^6}\left(1 - \frac{1}{2^7}\right)\langle v_{Fi}v_{Fj}v_{Fk}v_{Fl}v_{Fm}v_{Fn}\rangle \times (\Pi_i\Pi_j\Pi_k\Delta)^*(\Pi_l\Pi_m\Pi_n\Delta). \qquad (13)$$

Setting the z-axis perpendicular to the basal plane, the above terms can be split into isotropic in-plane part

$$F_6^{\rm iso} = K_6^i\Delta^*\left[\Pi_x^2 + \Pi_y^2\right]^3\Delta \qquad (14)$$

with $K_6^i = \frac{\zeta(7)N}{64\pi^6 T_c^6}\left(1 - \frac{1}{2^7}\right)\left(\langle v_{Fx}^6\rangle + \langle v_{Fy}^6\rangle\right)$, and anisotropic in-plane contribution

$$F_6^{\rm an} = \frac{1}{2}K_6^a\Delta^*\left[(\Pi_x + i\Pi_y)^6 + (\Pi_x - i\Pi_y)^6\right]\Delta \qquad (15)$$

with $K_6^a = \frac{\zeta(7)N}{64\pi^6 T_c^6}\left(1 - \frac{1}{2^7}\right)\left(\langle v_{Fx}^6\rangle - \langle v_{Fy}^6\rangle\right)$. This expression of $F_6^{\rm an}$ assumes that the x- and the y-axes are parallel to the reflection lines in the ab-plane. With the x-axis

parallel to the b-direction, tight-biding calculations [18] yield $\langle v_{Fx}^6\rangle = 4.608$, $\langle v_{Fy}^6\rangle = 4.601$ for the σ-band, while for the π-band, $\langle v_{Fx}^6\rangle = 1.514$, $\langle v_{Fy}^6\rangle = 1.776$ in units of 10^{46} (cm/s)^6. The different sign of the hexagonal harmonics of the Fermi velocities in the two bands is responsible for a unique 30-degree orientational transition of the vortex lattice in MgB_2 [18]. No theory can describe at present the electron-phonon effect on the hexagonal modulation of the Fermi surface. We use, therefore, the raw LDA values for all gradient coefficients in the consideration below. If we rotate now the orthogonal axes so that the y-axis is parallel to the magnetic field $\mathbf{H}$ when the latter forms an angle ϕ with the a-axis, the terms in F_6 change in a simple way: $F_6^{\rm iso}$ is preserved while $F_6^{\rm an}$ turns into

$$F_6^{\rm an} = \frac{1}{2}K_6^a\Delta^*\left[e^{i6\phi}(\Pi_x+i\Pi_y)^6 + e^{-i6\phi}(\Pi_x-i\Pi_y)^6\right]\Delta. \quad (16)$$

Since $\Pi_y = 0$, the extra term can be written as $F_6 = \sum K_{6,n}\Delta_n^*\Pi_x^6\Delta_n$ with $K_{6,n} = K_{6,n}^i + K_{6,n}^a\cos(6\phi)$. For the variational approximation, the new functional yields the quadratic form

$$F_2 = \left(\alpha_1 + \tilde{K}_1 h + \tilde{K}_{6,1}h^3\right)|c|^2 + \left(\alpha_2 + \tilde{K}_2 h + \tilde{K}_{6,2}h^3\right)|d|^2 - \tilde{\gamma}\,(c^*d + d^*c) \quad (17)$$

with $\tilde{K}_{6,n} = \frac{15}{8}K_{6,n}\mu_n^3$. While in the expansion method, this results in the new matrix element

$$M_{2p+n,2q+n'}^{F_2+F_6} = M_{2p+n,2q+n'}^{F_2} + h^3K_{6,n}\left(\frac{K_{nc}}{K_n}\right)^{3/2}M_{2p,2q}^{(6)}\delta_{n,n'} \quad (18)$$

with $M_{p,q}^{(6)} = \frac{1}{8}\langle\Psi_p|(\hat{a}^\dagger+\hat{a})^6|\Psi_q\rangle$ where $\hat{a}$ is the annihilation operator of Landau levels.

In the weakly anisotropic regime $F_6 \ll F_2$, we expect

$$H_{c2}(\phi) \approx H_{c2}^\circ\left(1+\eta^i+\eta^a\cos(6\phi)\right). \quad (19)$$

The isotropic parts yield a ϕ-independent shift of H_{c2} (and ensure $K_{6,n} > 0$ for the numerical solution converging) while the anisotropic parts are responsible for the six-fold modulation of the correction. η^a can change sign when the temperature varies because the anisotropies in each band are opposite. Figure 5 displays the corrections brought by the isotropic parts of F_6. The deviations become important below 30 K as expected out of the estimated GL regime, which implies the necessity to retain higher order terms in the gradient expansion of the GL functional.

The extra h^3 terms prevent from deriving an analytical expression for the magnetic field correction $\delta h_{c2} = h_{c2}(\phi) - h_{c2}(\pi/12)$. We can however partially estimate the latter. Let us name the quantities related to the quadratic form $(F_2 + F_6^{\rm iso})$ with the superscript "$\circ$", and the ones for $(F_2 + F_6^{\rm iso} + F_6^{\rm an})$ without it. Within the variational

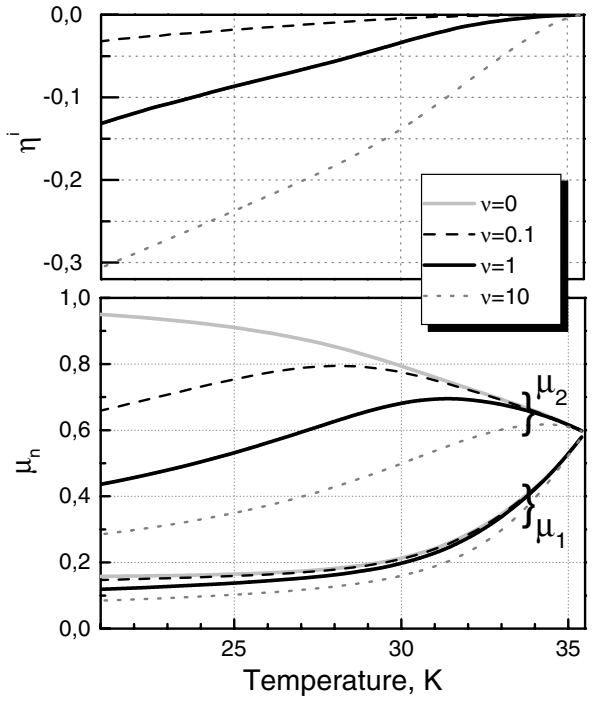

Fig. 5. Influence of the isotropic correction F_6 with $(\langle v_{F1}^6\rangle, \langle v_{F2}^6\rangle) = \nu(4.6, 1.6)$ (in units of 10^{46} (cm/s)^6) for different magnitudes ν: relative shift of the upper critical field $\eta^i = (H_{c2}^\nu - H_{c2}^\circ)/H_{c2}^\circ$ and corresponding variational parameters μ_n.

method, we then find with a perturbation expansion

$$\frac{\delta\tilde{h}_{c2}}{\tilde{h}_{c2}^\circ} \approx \frac{1}{\tilde{h}_{c2}^\circ}\frac{d\tilde{h}_{c2}^\circ}{dT}\left.\frac{\langle\Delta^\circ|F_6^{\rm an}|\Delta^\circ\rangle}{\langle\Delta^\circ|\partial(F_2+F_6^{\rm iso})/\partial T|\Delta^\circ\rangle}\right|_{\tilde{h}_{c2}^\circ} \quad (20)$$

$$\approx \frac{15}{8}\cos(6\phi)T\frac{d\tilde{h}_{c2}^\circ}{dT}{\tilde{h}_{c2}^\circ}^2\frac{K_{6,1}^a{\mu_1^\circ}^3 + K_{6,2}^a{\mu_2^\circ}^3\rho^2}{a_1+a_2\rho^2}$$

where $\rho^2 = |c^\circ/d^\circ|^2$. The expansion method provides in a similar way

$$\frac{\delta h_{c2}}{h_{c2}^\circ} \approx \frac{T}{h_{c2}^\circ}\frac{dh_{c2}^\circ}{dT}\left.\frac{(1+\rho^2)\langle\Delta^\circ|F_6^{\rm an}|\Delta^\circ\rangle}{a_1+a_2\rho^2}\right|_{h_{c2}^\circ} \quad (21)$$

but $\langle\Delta^\circ|F_6^{\rm an}|\Delta^\circ\rangle$ has a more complicated expression.

In Figure 6, we have plotted the relative modulation amplitude $\eta^a = (h_{c2}(0) - h_{c2}(\pi/6))/(h_{c2}(0) + h_{c2}(\pi/6))$ with the hexagonal anisotropy $\langle v_{Fb}^6\rangle = \langle v_F^6\rangle^i + \langle v_F^6\rangle^a$ and $\langle v_{Fa}^6\rangle = \langle v_F^6\rangle^i - \langle v_F^6\rangle^a$ where $(\langle v_{F1}^6\rangle^i, \langle v_{F2}^6\rangle^i) = (4.6, 1.6)$ while $(\langle v_{F1}^6\rangle^a, \langle v_{F2}^6\rangle^a) = (0.3\nu_1, -0.2\nu_2)$ (in units of 10^{46} (cm/s)^6). Ab initio calculations provides $\langle v_{F1}^6\rangle^a \ll \langle v_{F2}^6\rangle^a$ for MgB_2 which corresponds around to the couple $(\nu_1, \nu_2) = (0; 1)$ in Figure 6. Due to the LDA results uncertainty and also to illustrate the interplay between the two bands, the plots for other values of (ν_1, ν_2) are displayed. Note the results at low temperature should be taken with caution since they are obtained out of the GL regime. When the hexagonal anisotropies of each band

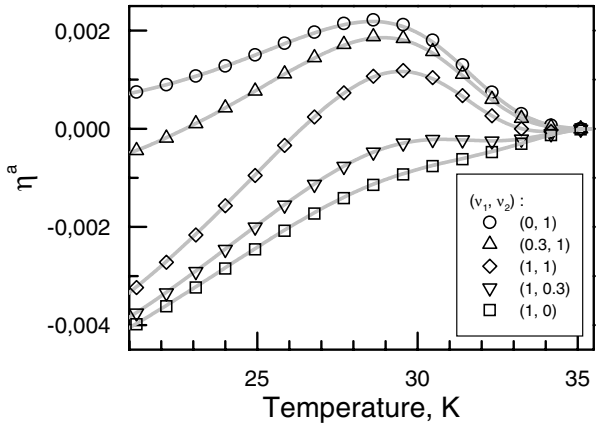

Fig. 6. Relative modulation amplitude for different pairs (ν_1, ν_2): solid lines are obtained with the variational method and symbols with estimate (20).

are of the same order, η^a sign can change with temperature. But this modulation is too small to be detected experimentally in the GL regime, which agrees with measurements reported by Shi et al. [8]. Estimation (20) gives three reasons for this. First, η^a grows as h_{c2}^2 contrary to the four-fold symmetry crystal case where the increase is linear. Then the anisotropies of the two bands oppose each other. And finally, even though $\langle v_{F1}^6 \rangle^a$ would be too small to compete with $\langle v_{F2}^6 \rangle^a$, the contribution from the second band is reduced by the rapidly decreasing factor ρ^2 and, below 30 K, by μ_2^3.

5 Conclusions

Angular and temperature dependence of the upper critical field of MgB_2 have been determined within the two-gap GL theory. We have used two different numerical methods which are in excellent agreement with each other and yield an unconventional anisotropy of H_{c2} observed in the superconductor MgB_2. Such a behavior reflects the different Fermi sheet geometries and the varying importance of the small π-gap. The zeroth Landau levels employed in the variational approach are sufficient for accurate description of the continuous transition at H_{c2}. Contrary to the single-gap case, spatial anisotropy of the gap functions in the plane perpendicular to the magnetic field changes with temperature and can be different for each band. This explains the deviation from the effective mass angular dependence (12) applicable to ordinary superconductors. Existence of two different characteristic lengths should also affect the vortex core shape [18], especially when an applied field is perpendicular to the c-axis. The gap functions have an effective single-component behavior only in a temperature region near T_c significantly narrower than the range for the validity of the two-gap GL theory $\sim (T_c - T)/T_c \sim 1/7$. At last, the hexagonal ab-plane modulation of H_{c2} arising from the crystal symmetry can result in a change of the sign of the hexagonal harmonics of $H_{c2}(\theta)$ when the temperature is decreased.

References

1. H. Suhl, B.T. Matthias, L.R. Walker, Phys. Rev. Lett. **3**, 552 (1959)
2. V.A. Moskalenko, Fiz. Met. Metalloved. **8**, 503 (1959) [Sov. Phys. Met. Matallogr. **8**, 25 (1959)]
3. J. Nagamatsu, N. Nakagawa, T. Muranaka, Y. Zenitani, J. Akimitsu, Nature **410**, 63 (2001)
4. See for review on MgB_2 the special issue Physica C **385**, 1-305 (2003)
5. M. Angst, R. Puzniak, A. Wisniewski, J. Jun, S.M. Kasakov, J. Karpinski, J. Roos, H. Keller, Phys. Rev. Lett. **88**, 167004 (2002)
6. L. Lyard, P. Samuely, P. Szabo, T. Klein, C. Marcenat, L. Paulius, K.H.P. Kim, C.U. Jung, H.-S. Lee, B. Kang, S. Choi, S.-I. Lee, J. Marcus, S. Blanchard, A.G.M. Jansen, U. Welp, G. Karapetrov, W.K. Kwok, Phys. Rev. B **66**, 180502 (2002)
7. R. Cubitt, S. Levett, S.L. Bud'ko, N.E. Anderson, P.C. Canfield, Phys. Rev. Lett. **90**, 157002 (2003)
8. Z.X. Shi, M. Tokunaga, T. Tamegai, Y. Takano, K. Togano, H. Kito, H. Ihara, Phys. Rev. B **68**, 104513 (2003)
9. A. Rydh, U. Welp, A.E. Koshelev, W.K. Kwok, G.W. Crabtree, R. Brusetti, L. Lyard, T. Klein, C. Marcenat, B. Kang, K.H. Kim, K.H.P. Kim, H.-S. Lee, S.-I. Lee, Phys. Rev. B **70**, 132503 (2004)
10. A.A. Golubov, A. Brinkman, O.V. Dolgov, J. Kortus, O. Jepsen, Phys. Rev. B **66**, 054524 (2002)
11. A.A. Golubov, A.E. Koshelev, Phys. Rev. B **68**, 104503 (2003)
12. P. Miranovic, K. Machida, V.G. Kogan, J. Phys. Soc. Jpn **72**, 221 (2003)
13. V.G. Kogan, S.L. Bud'ko, Physica C **385**, 131-142 (2003)
14. T. Dahm, N. Schopohl, Phys. Rev. Lett. **91**, 017001 (2003)
15. A. Gurevich, Phys. Rev. B **67**, 184515 (2003)
16. M. Arai, T. Kita, J. Phys. Soc. Jpn **73**, 2924 (2004)
17. R. Cubitt, M.R. Eskildsen, C.D. Dewhurst, J. Jun, S.M. Kazakov, J. Karpinski, Phys. Rev. Lett. **91**, 047002 (2003)
18. M.E. Zhitomirsky, V.H. Dao, Phys. Rev. B **69**, 054508 (2004)
19. D.R. Tilley, Proc. Phys. Soc. **84**, 573 (1964)
20. B.T. Geilikman, R.O. Zaitsev, V.Z. Kresin, Fiz. Tverd. Tela **9**, 821 (1967) [Sov. Phys. Solid State **9**, 642 (1967)]
21. Y. Kong, O.V. Dolgov, O. Jepsen, O.K. Andersen, Phys. Rev. B **64**, 020501 (2001)
22. I.I. Mazin, V.P. Antropov, Physica C **385**, 49 (2003)
23. I.I. Mazin, O.K. Andersen, O. Jepsen, O.V. Dolgov, J. Kortus, A.A. Golubov, A.B. Kuz'menko, D. van der Marel, Phys. Rev. Lett. **89**, 107002 (2002)
24. S.V. Pokrovsky, V.L. Pokrovsky, Phys. Rev. B **54**, 13275 (1996)
25. M.R. Skokan, R.C. Morris, W.G. Moulton, Phys. Rev. B **13**, 1077 (1976)
26. P.C. Hohenberg, N.R. Werthamer, Phys. Rev. **153**, 493 (1967)
27. K. Takanaka, Prog. Theor. Phys. **46**, 1301 (1971)